Evolution of hyperossification expands skull diversity in frogs

Daniel J. Paluh[a,b,1] , Edward L. Stanley[a] , and David C. Blackburn[a]

[a]Department of Natural History, Florida Museum of Natural History, University of Florida, Gainesville, FL 32611; and [b]Department of Biology, University of Florida, Gainesville, FL 32611

Frogs (Anura) are one of the most diverse vertebrate orders, comprising more than 7,000 species with a worldwide distribution and extensive ecological diversity. In contrast to other tetrapods, frogs have a highly derived body plan and simplified skull. In many lineages of anurans, increased mineralization has led to hyperossified skulls, but the function of this trait and its relationship with other aspects of head morphology are largely unexplored. Using three-dimensional morphological data from 158 species representing all frog families, we assessed wide-scale patterns of shape variation across all major lineages, reconstructed the evolutionary history of cranial hyperossification across the anuran phylogeny, and tested for relationships between ecology, skull shape, and hyperossification. Although many frogs share a conserved skull shape, several extreme forms have repeatedly evolved that commonly are associated with hyperossification, which has evolved independently more than 25 times. Variation in cranial shape is not explained by phylogenetic relatedness but is correlated with shifts in body size and ecology. The species with highly divergent, hyperossified skulls often have a specialized diet or a unique predator defense mechanism. Thus, the evolution of hyperossification has repeatedly facilitated the expansion of the head into multiple new shapes and functions.

Anura | cranium | dermal ornamentation | geometric morphometrics | microcomputed tomography

Identifying the factors that drive evolutionary changes in the heads of vertebrates has been a long-standing challenge because of the difficulties of sampling taxa broadly, quantifying complex morphologies, and identifying possible mechanisms responsible for generating macroevolutionary patterns. The diverse selective pressures proposed to drive extreme derivations in the skull include specializations in feeding biology (1), habitat use (2), and locomotion (3). Sexual selection also is thought to influence head morphology because the skull often is sexually dimorphic in size and shape (4, 5). The interactions among these selective pressures can result in functional trade-offs (6) that shape the head as an integrated system that must house the sensory organs, capture prey, provide protection, and partake in locomotion and reproduction (7). The nonadaptive mechanisms of architectural constraint (i.e., allometry; ref. 8) and phylogenetic conservatism (9) also have been invoked to explain morphological variation within and across lineages, particularly in cases in which extreme shifts are absent. The diversification of the skull usually results from changes in size or shape of preexisting elements or the loss of bones (10), but the origin of novel structures also may be responsible for shifts in morphology (11).

Increased mineralization or hyperossification of the skull is a recurrent feature among vertebrates; it also is known as dermal ornamentation (12, 13). In its most rudimentary form, additional membrane bone is deposited on the skeleton to form ridges and crests that produce a reticulate or pitting pattern on the surface of bones (exostosis), but, in extreme cases, hyperossification can lead to the formation of helmet-like protuberances (casquing) or coossification between the skeleton and dermis (14). Hyperossification is thought to result from the heterochronic process of

peramorphosis, which is the extension or acceleration of ancestral ontogenetic trajectories (15). Despite its widespread occurrence in actinopterygians, amphibians, and amniotes, the functional role of hyperossification and its relationship with other aspects of head morphology, such as skull shape, are largely unexplored.

Skull evolution has been poorly studied using contemporary methods in anurans (frogs and toads) relative to more species-poor lineages [e.g., carnivoran mammals (1, 16) and crocodilians (17, 18)]. Frog skulls may be understudied because it has been assumed that the highly derived Bauplan and skeletal morphology of this clade are tightly conserved (19). The work of Trueb (14) represents the only comprehensive description of skull osteology in anurans, but the number of described species has more than doubled since its publication [3,260 species in 1979 (20), 7,165 species in 2020 (21)], and our understanding of the anuran tree of life has fundamentally changed with the development of molecular phylogenetics (22–24). Frog skull anatomy is generally thought to be correlated with body size (25), feeding biology (26), and microhabitat use [e.g., terrestrial, aquatic, fossorial (14, 27)]. Most anurans have a simplified skull [due to the reduced number of cranial elements relative to other amphibians (22)] that acts as a supporting scaffold for the sensory organs of the head (28), but some species possess increased ossification [e.g., some bufonid toads, casque-headed hylids (22)]. Cranial hyperossification is

Significance

The vertebrate head is an integrated system essential for sensory functions, capturing prey, and defense mechanisms. Head anatomy has long attracted the attention of biologists, yet identifying the factors responsible for the evolution of deviant morphological forms has remained a long-standing challenge. Frogs are one of the most diverse vertebrate orders but have not been thoroughly studied with respect to cranial morphological variation. We use extensive sampling of all major lineages to quantify skull diversity, reconstruct the evolution of increased mineralization (hyperossification), and test for relationships between ecology, skull shape, and hyperossification. We find that several extreme skull shapes have repeatedly evolved in frogs, hyperossification has arisen independently many times, and deviant skulls often cooccur with hyperossification and specialized functions.

expressed on five dermal elements (frontoparietal, nasal, premaxilla, maxilla, squamosal) and three novel bones (prenasal, internasal, dermal sphenethmoid) in frogs (29). Although hyperossification has been described in a diversity of taxa, there have been no attempts to test the number of origins of this trait or its function(s) in extant anurans. Increased mineralization has been hypothesized to aid in the prevention of evaporative water loss in arid microhabitats (14, 30), strengthen the skull for catching large prey (27), or reinforce the skull for protection against predators in frogs that use their heads to fill cavities or block holes [termed phragmotic behavior (27, 29)]. Alternately, hyperossification may arise as a byproduct of miniaturization (31).

Using the most recent species-rich phylogeny of extant amphibian species (32) and extensive taxonomic sampling via high-resolution X-ray microcomputed tomography (158 species representing all 54 described anuran families), we 1) evaluated the broad-scale patterns of skull shape diversity across all major frog lineages, 2) reconstructed the evolutionary history of skull hyperossification, and 3) tested the ways in which body size, feeding biology, microhabitat use, and phragmotic defense behavior are associated with skull shape and interact with hyperossification. Our results demonstrate that, although many lineages share a conserved skull shape, several highly divergent skull architectures have evolved repeatedly throughout the evolutionary history of frogs. Hyperossification has evolved independently many times and often cooccurs with divergent skull shapes. Body size, microhabitat use, and feeding biology are each correlated with variation in head shapes, and vertebrate predation and phragmotic defense behavior cooccur with hyperossification and extreme skull shapes.

Results

Diversity in Skull Shape. We used three-dimensional (3D) geometric morphometric analyses on 36 fixed landmarks (*SI Appendix*, Fig. S1) in the R package geomorph version 3.0.3 (33) to quantify shape variation among skulls from all major lineages of frogs (Fig. 1). The PC1 axis (21% of variation) primarily describes shape differences driven by the relative position of the jaw joint, relative length and width of the frontoparietal, relative height of the skull, and shape of the snout in dorsal view (Fig. 2, skulls A and B). The PC2 axis (16%) primarily describes shape differences driven by the relative size of squamosal and its processes (zygomatic ramus [anterior process] and otic ramus [posterior process]), relative height of the skull, and relative width of the skull (Fig. 2, skulls C and D). The PC3 axis (11%) primarily describes shape differences driven by the degree of fenestration on the skull roof (Fig. 2, skulls E and F). There is significant phylogenetic signal in skull shape among the frogs in our dataset, but less than expected under a Brownian Motion model of evolution ($K_{mult} = 0.52$, $P < 0.005$). The species approaching the minimum and maximum values of PC1 to PC3 are dispersed throughout the phylogeny (Fig. 1 and *SI Appendix*, Fig. S2), indicating that highly divergent shapes have evolved repeatedly. There is no support for phylogenetic signal in skull centroid size ($K_{mult} = 0.42$, $P = 0.07$). A phylogenetic regression indicated there is a positive size to shape relationship (degree of freedom [df], 1; sum of squares [SS], 0.004845; means square [MS], 0.004845; R^2, 0.09035; F-ratio [F], 15.494; Z score [Z], 7.0476; $P < 0.005$; Fig. 3A); small species possess relatively large braincases and sensory capsules in contrast to large species, which have small braincases and expanded dermal elements.

Ancestral Reconstruction of Hyperossification. Hyperossification occurs in 44 of the 158 anuran taxa in our dataset and is distributed across 39 genera and 17 families (Fig. 1). We used reversible-jump Markov chain Monte Carlo (MCMC) in RevBayes (34) to sample all five Markov models of phenotypic character evolution in proportion to their posterior probability, and the maximum a

posteriori model of hyperossification evolution was the one-rate model with a posterior probability of 0.9 (*SI Appendix*, Table S1). This model is strongly supported over the two-rate model (Bayes factor = 10.45) and both irreversible models (Bayes factors > 100; *SI Appendix*, Table S1). The model-averaged maximum a posteriori ancestral state of frogs was nonhyperossified with a posterior probability of 0.99. Hyperossification arose independently 30 times over the phylogeny, and one reversal from hyperossified to nonhyperossified was inferred (Fig. 1). Hyperossification has originated 3 times in Mesobatrachia, 8 times in Ranoidea, 18 times in Hyloidea, and once in Calyptocephalellidae.

Ecology, Skull Shape, and Hyperossification. Phylogenetic multivariate analysis of variance (MANOVA) tests indicate that a significant relationship exists between microhabitat use (aquatic, arboreal, fossorial, terrestrial) and skull shape (df, 3; SS, 0.002909; MS, 0.0009676; R^2, 0.05425; F, 2.9447; Z, 4.8252; $P < 0.005$; Fig. 2 A and B), feeding biology (invertebrate predator, vertebrate predator) and skull shape (df, 1; SS, 0.002078; MS, 0.00207767; R^2, 0.03846; F, 6.2877; Z, 5.0498; $P < 0.005$; Fig. 2 C and D), and phragmotic behavior (present, absent) and skull shape (df, 1; SS, 0.001764; MS, 0.00176366; R^2, 0.03289; F, 5.3051; Z, 4.3166; $P < 0.005$; Fig. 2 A and B). Post hoc pairwise comparisons suggest all microhabitat categories significantly differ from one another in mean skull shape (*SI Appendix*, Table S2). There are no differences in morphological disparity between hyperossified species and nonhyperossified species ($P = 0.14$; nonhyperossified [NH] Procrustes variance, 0.0261; hyperossified [H] Procrustes variance, 0.0318), but there is a significant difference in the net rate of morphological evolution between the two groups (observed rate ratio, 1.75; $P = 0.0001$), with hyperossified species phenotypically evolving at twice the rate of nonhyperossified species (NH rate, 2.60×10^{-6}; H rate, 4.56×10^{-6}). A phylogenetic MANOVA indicates that the mean skull shape of hyperossified species and nonhyperossified species differs (df, 1; SS, 0.003657; MS, 0.0036575; R^2, 0.0682; F, 11.419; Z, 6.7622; $P < 0.005$), thereby suggesting that hyperossification is associated with shifts in skull morphology (Figs. 1 and 2). A factor interaction and homogeneity of slopes test indicated there is no interaction between hyperossification and skull size (residual degree of freedom [ResDf], 154; residual sum of squares [RSS], 0.044520; SS, 0.00035929; MS, 0.00035929; R^2, 0.0067; F, 1.2428; Z, 0.77042; $P = 0.22018$; Fig. 3A) and no difference in allometric slope vector length ($P = 0.40$) or angle ($P = 0.22$) between hyperossified and nonhyperossified species (Fig. 3A).

There is a significant factor interaction between hyperossification and microhabitat after accounting for each main effect (ResDf, 150; RSS, 0.044780; SS, 0.0022117; MS, 0.00073725; R^2, 0.041245; F, 2.4695; Z, 3.8373; $P < 0.005$; Fig. 2 A and B). Post hoc pairwise comparisons indicate that the interaction is primarily driven by differences in skull shape between hyperossified terrestrial frogs and nonhyperossified terrestrial frogs and differences in skull shape between hyperossified terrestrial frogs and hyperossified arboreal frogs (*SI Appendix*, Table S3). A significant factor interaction was found between hyperossification and feeding biology (ResDf, 154; RSS, 0.047777; SS, 0.00086747; MS, 0.00086747; R^2, 0.016177; F, 2.7961; Z, 3.0178; $P < 0.005$; Fig. 2 C and D), and post hoc pairwise comparisons reveal that the interaction is driven by the difference in skull shape between hyperossified vertebrate predators and nonhyperossified vertebrate predators (*SI Appendix*, Table S4). Odontoid fangs were recorded on the mandibles of 11 species (of the 158 examined), and true mandibular teeth were identified in one species (Fig. 1 and *SI Appendix*). Nine of the 11 taxa with odontoid fangs are hyperossified vertebrate predators (Dataset S1). All known anuran species that exhibit phragmotic defense behavior also are
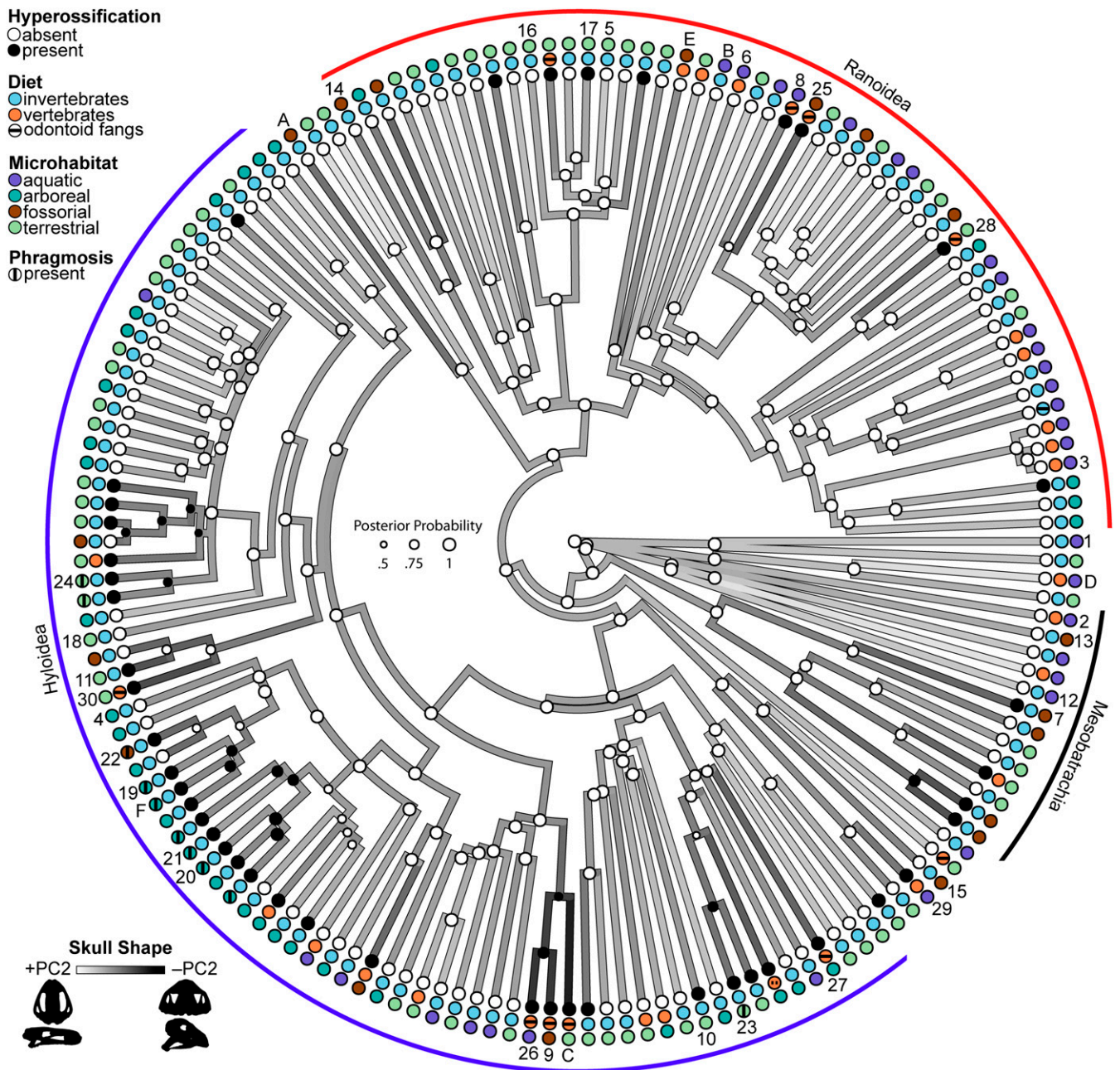
Fig. 1. Phylogenetic tree of frogs depicting the evolution of skull shape and hyperossification. Branch color gradient corresponds to maximum likelihood ancestral states of skull shape (PC2): Lineages with positive scores (white) have a narrow and flat skull, whereas lineages with negative scores (black) have a wide and tall skull. Node point color corresponds to Bayesian model-averaged ancestral states of frog skull hyperossification: white, absent; black, present. The size of each node point represents the posterior probability of the most probable ancestral state. Tip point colors correspond to hyperossification, diet, and microhabitat states for all 158 species. A horizontal bar on the diet point indicates the presence of odontoid fangs, and a vertical bar on the microhabitat point indicates the presence of phragmotic behavior. Tip numbers 1 to 30 correspond to species depicted in Fig. 4, and tip letters A to F correspond to species depicted in Fig. 2. Species tip labels are provided in *SI Appendix*, Fig. S4, and corresponding trait data are provided in Dataset S1.

hyperossified; therefore, a factor interaction between the two traits is not possible.

Discussion

Diversity in Skull Shape. We identified substantial skull diversity across the 158 anuran species examined (Fig. 4). Phylogenetic relatedness does not explain variation in the skull, as demonstrated by several lineages convergently evolving similar extreme shapes (Fig. 2 *A* and *B*). A significant allometric relationship characterizes all frog skulls in our dataset. Small anurans possess

a large braincase and reduced dermatocranium (e.g., *Paedophryne swiftorum*; Fig. 4, skull 5) compared to large species (e.g., *Conraua goliath*; Fig. 4, skull 6), a pattern that has been previously found in frogs (35). The relatively large braincase and sensory capsules observed in miniaturized species suggests the neurocranium may have a critical minimum, constrained to be large enough to accommodate the brain and sensory organs. Skull shapes differ among frogs that occupy distinct microhabitats. Fossorial and aquatic species are nearly nonoverlapping in morphospace (Fig. 2 *A* and *B*), with fossorial species possessing short, tall skulls with an
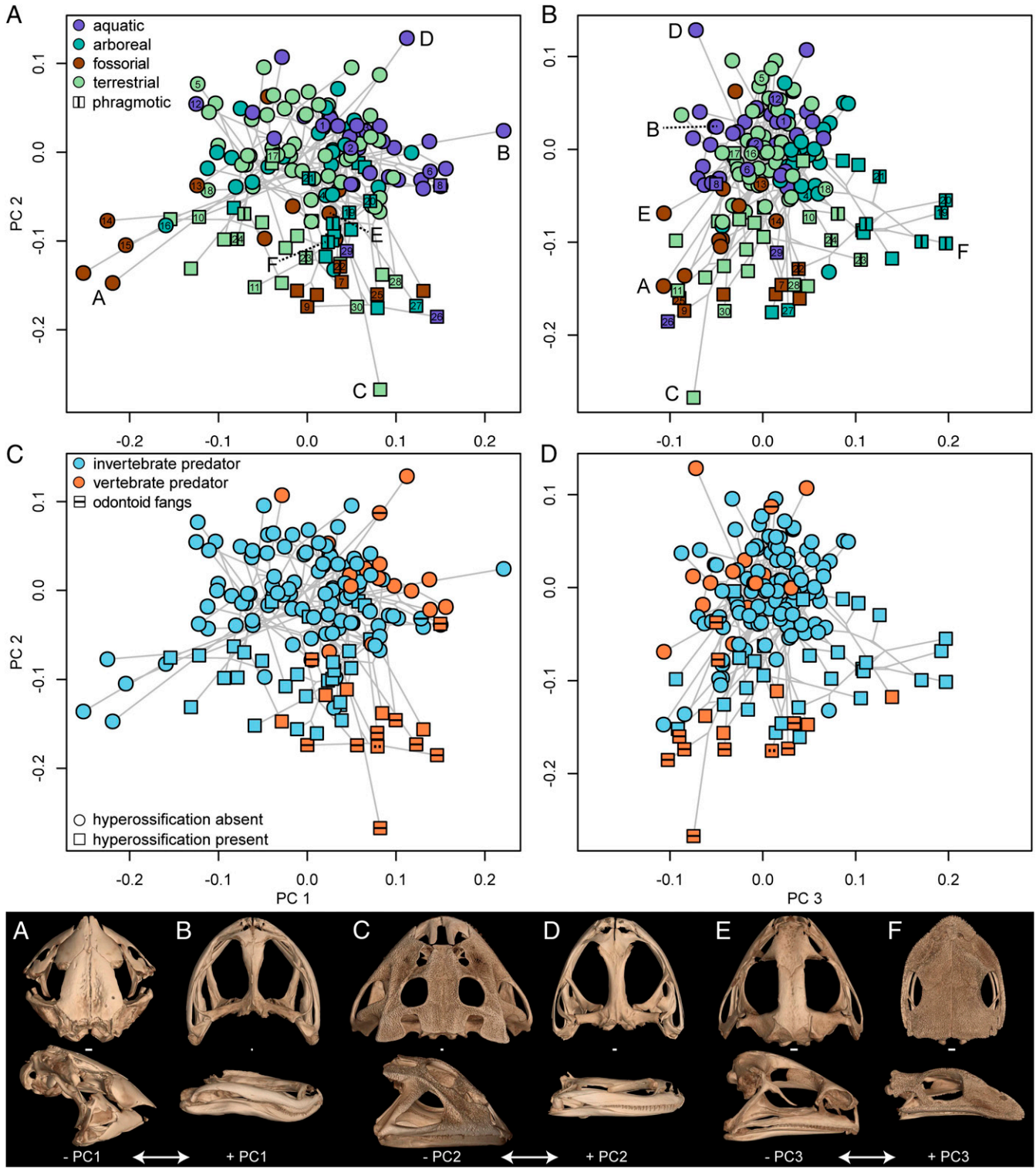
Fig. 2. Phylomorphospace plots of (*A* and *C*) PC1 and PC2 and (*B* and *D*) PC2 and PC3 axes of shape variation exhibiting the diversity of skull morphology in frogs. Square points, hyperossification present; circle points, hyperossification absent. Points are colored by (*A* and *B*) microhabitat and (*C* and *D*) diet states. Point numbers 1 to 30 correspond to species in Fig. 4. Skulls A to F are species approaching the minimum and maximum PC shape scores for each axis of variation: skull A, *Nasikabatrachus sahyadrensis* (CESF 203; −PC1); skull B, *Conraua beccarii* (TNHC 37720; +PC1); skull C, *Ceratophrys aurita* (CAS 84998; −PC2); skull D, *Barbourula busuangensis* (UF 70546; +PC2); skull E, *Hildebrandtia ornata* (CAS 154657; −PC3); and skull F, *Triprion petasatus* (UF 98441; +PC3). (Scale bar, 1 mm.) Species labels for all points are provided in *SI Appendix*, Fig. S5.

anterior jaw joint (+PC1; Fig. 2, skull A and Fig. 3*B*) and aquatic taxa possessing an elongate, flattened skull with a posterior jaw joint (−PC1; Fig. 2, skull B and Fig. 3*B*). We found a significant

difference in skull shape between frogs that prey on vertebrates and those only known to eat invertebrates (Fig. 2 *C* and *D*). Most species capable of eating vertebrate prey have a relatively tall skull
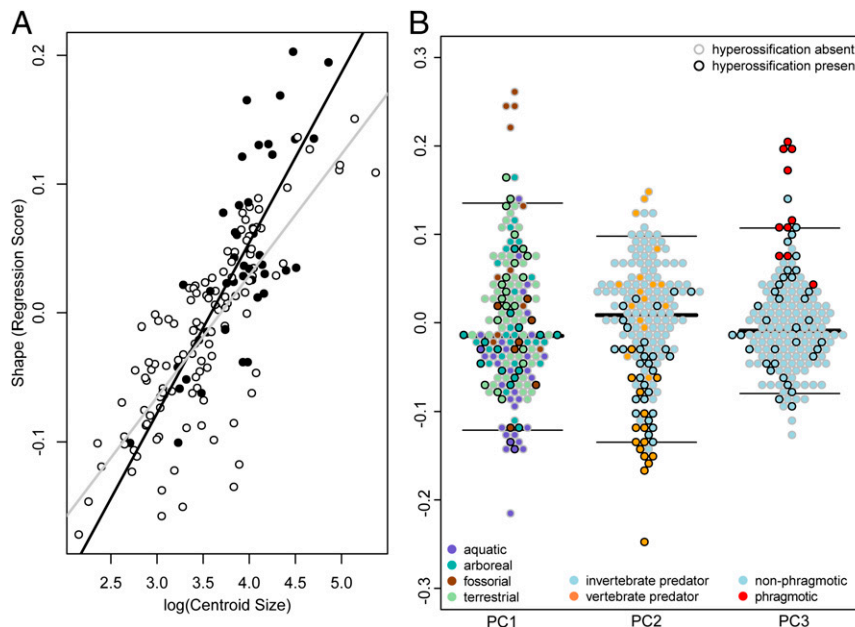
Fig. 3. (A) Multivariate regression between skull shape (RegScore) and skull centroid size. Ordinary least-squares regression lines are displayed for hyperossified species (black points, black line) and nonhyperossified species (white points, gray dashed line) to demonstrate the lack of slope differences between these two groups (see diversity in skull shape in results). Species labels for all points are provided in *SI Appendix*, Fig. S6. (B) Beeswarm plots (67) of PC scores illustrating highly divergent shapes are associated with fossorial and aquatic microhabitats (PC1), vertebrate predation (PC2), and phragmotic behavior (PC3). Black outline, hyperossification present; gray outline, hyperossification absent. Median and 95% CI lines are shown for each PC score.

with a posteriorly shifted jaw joint, which allows for a large gape (Fig. 2, skull C and ref. 26). A highly divergent region of morphospace is occupied by myrmecophagous specialists (diet of ants and termites) that have converged on a skull shape characterized by a pointed, short snout, anteriorly shifted jaw point, reduced squamosal, and a tall skull (e.g., *Rhinophrynus dorsalis*, *Hemisus guttatus*, *Myobatrachus gouldii*; Fig. 4, skulls 13 to 18). This extreme head shape is likely driven more by diet than a burrowing locomotory mode, as Vidal-Garcia and Keogh (9) demonstrated that among burrowing myobatrachid frogs, only ant and termite specialists have a short, pointed snout. The tongueless pipid frogs have a bizarre, flattened skull (e.g., *Pipa parva*; Fig. 4, skull 12; ref. 36), which is tightly linked to their derived mechanism of catching prey under water through suction feeding (37, 38).

Evolution of Hyperossification. Hyperossification occurs in diverse frog lineages and has arisen independently over 25 times in living anurans. The absence of hyperossification at the root of frogs is supported by the fossil record because all known stem salientians with cranial material lack hyperossification [*Triadobatrachus* (39), *Prosalirus* (40), *Vieraella* (41), *Liaobatrachus* (42)]. Hyperossified species have higher rates of skull shape evolution as compared to nonhyperossified species, which suggests that hyperossified frogs can quickly invade into novel regions of morphospace. This is also consistent with the hypothesis that hyperossification is a peramorphic trait (31) that may be associated with accelerated ontogenetic trajectories and morphological change (15, 43). The mean shape of hyperossified frogs differs significantly from that of nonhyperossified taxa, but, as a group, they are not more variable (i.e., disparate). Hyperossified lineages have evolved at least two highly divergent skull shapes (extreme −PC2 space, extreme +PC3 space; Fig. 3B), and, when viewed in phylomorphospace, there is evidence of repeated or convergent evolution because distantly related taxa are found in close proximity. Multiple disparate functional pressures unrelated to body size may be associated with the evolution of hyperossification (see below). The skulls of both nonhyperossified and hyperossified anurans have the same allometric

slopes (Fig. 3A); thus, hyperossification does not evolve as a byproduct of miniaturization. Hyperossification is present in both miniaturized and gigantic species (ranging from 5 mm [*Brachycephalus ephippium*, Fig. 4, skull 10] to 56 mm [*Ceratophrys aurita*, Fig. 2, skull C] in head length), as well as many intermediate-sized taxa. Within extant anurans, both the smallest (*Paedophryne*; Fig. 4, skull 5) and largest (*Conraua goliath*; Fig. 4, skull 6) frogs lack hyperossification; however, the largest crown-group fossil frog described, *Beelzebufo ampinga* from the Late Cretaceous (44), is hyperossified.

Microhabitat Use. Hyperossified frogs can be found in all microhabitats, but the relative frequency of the trait is lower in aquatic frogs (3/33 species, 9%) than the other categories (arboreal: 14/38, 37%; fossorial: 7/18, 39%; terrestrial: 20/69, 29%; Dataset S1). The broad distribution of microhabitats used by hyperossified lineages suggests that hyperossification is not strictly associated with arid environments. Furthermore, many arid-adapted fossorial genera (e.g., *Breviceps*, *Myobatrachus*) lack hyperossification (*SI Appendix*). We identified an interaction between hyperossification and microhabitat use driven by differences in skull shape between hyperossified terrestrial frogs and nonhyperossified terrestrial frogs and differences between hyperossified terrestrial frogs and hyperossified arboreal frogs. Nonhyperossified and hyperossified terrestrial frogs are largely separated by the PC2 axis of shape variation (Fig. 2A), with nonhyperossified terrestrial frogs having flatter, narrower skulls with a shorter zygomatic ramus of the squamosal. The shape difference between these two groups is likely not associated with using terrestrial habitats differently, but instead with diet (discussed below). Hyperossified terrestrial and hyperossified arboreal frogs are largely separated by the PC3 axis of shape variation (Fig. 2B), with hyperossified terrestrial frogs having narrower frontoparietals and larger orbital cavities. The expanded skull roof of hyperossified arboreal frogs may be linked to preventing evaporative water loss, as it has been demonstrated that the moisture gradient between the ground and canopy in tropical rainforests can be steeper than moisture gradients across elevations (45). Additionally, the rate of cutaneous evaporative
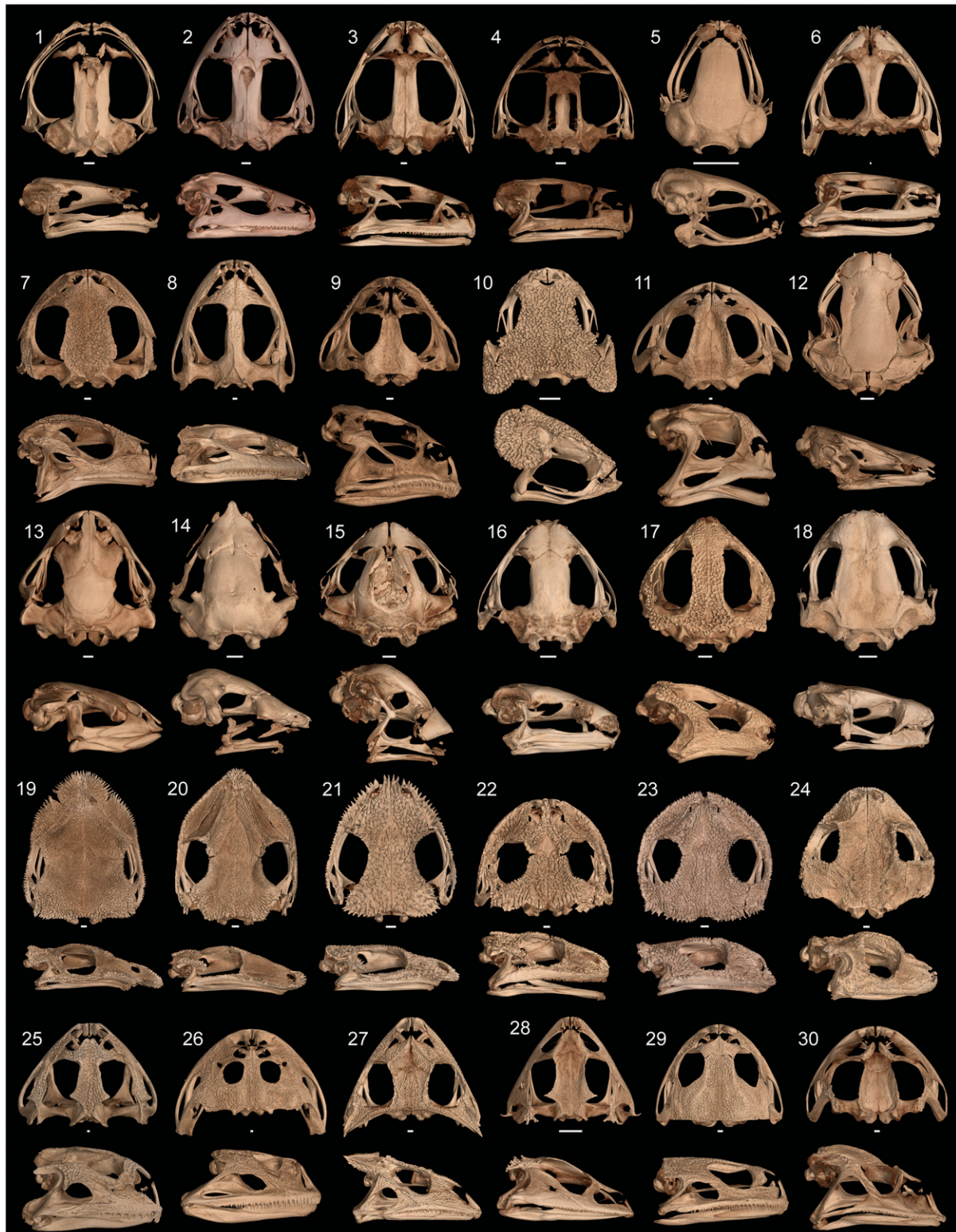
Fig. 4. Representative frog skulls used in this study depicting morphological diversity: 1, *Ascaphus truei* (UF 80664); 2, *Discoglossus pictus* (KU 144217); 3, *Rana clamitans* (UF 76511); 4, *Hyla chrysoscelis* (UF 64907); 5, *Paedophryne swiftorum* (BPBM 31884); 6, *Conraua goliath* (UF 64720); 7, *Scaphiopus holbrookii* (UF 9620); 8, *Aubria masako* (MCZ A-135999); 9, *Chacophrys pierottii* (KU 191932); 10, *Brachycephalus ephippium* (UF 72725); 11, *Macrogenioglottus alipioi* (USNM 200455); 12, *Pipa parva* (UF 37924); 13, *Rhinophrynus dorsalis* (CAS 71766); 14, *Hemisus guineensis* (CAS 258533); 15, *Myobatrachus gouldii* (MCZ A-139543); 16, *Copiula oxyrhina* (AMNH A-60046); 17, *Pherohapsis menziesi* (AMNH 8449); 18, *Melanophryniscus stelzneri* (UF 63183); 19, *Diaglena spatulata* (UF 109706); 20, *Aparasphenodon brunoi* (UF 71781); 21, *Corythomantis greeningi* (UF 92220); 22, *Smilisca fodiens* (KU 062348); 23, *Gastrotheca galeata* (KU 174361); 24, *Peltophryne guentheri* (UF 104862); 25, *Pyxicephalus adspersus* (UF 92093); 26, *Lepidobatrachus laevis* (UF 12347); 27, *Hemiphractus proboscideus* (CAS 122210); 28, *Ceratobatrachus guentheri* (UF 80585); 29, *Calyptocephalella gayi* (CAS 10082); 30, *Proceratophrys boiei* (CM 45985). (Scale bar, 1 mm.)

EVOLUTION

water loss from the head of a hyperossified arboreal hylid (*Trachycephalus jordani*) was found to be lower than in aquatic and arboreal nonhyperossified anurans [*Rana* and *Hyla*, respectively (30)]. Measuring the rate of water loss across a diversity of nonhyperossified and hyperossified anurans along microhabitat and microclimatic gradients is likely needed to further disentangle these relationships.

Feeding Biology. A significant interaction was found between hyperossification and feeding biology driven by the difference in skull shape between hyperossified vertebrate predators and nonhyperossified vertebrate predators. These groups are largely separated by the PC2 axis of shape variation (Figs. 2*C* and 3*B*), with hyperossified vertebrate predators having a wider, taller, and anteroposteriorly shorter skull with an enlarged squamosal. The zygomatic ramus of the squamosal is greatly expanded, forming a bony articulation with the posterior process of the maxilla, in 12 of the 14 hyperossified vertebrate predators (Fig. 2, skull C, Fig. 4, skulls 8 and 9 and skulls 25 to 30, and Dataset S1). Only one nonhyperossified species has a bony contact between the squamosal and maxilla (*Discoglossus pictus*; Fig. 4, skull 2), and a subset of hyperossified species not known to consume vertebrates also have this articulation (e.g., *Scaphiopus holbrookii*; Fig. 4, skull 7 and Dataset S1). Contact between the squamosal and maxilla forms a complete posterior margin to the orbit and not only strengthens the skull but also increases the size of the adductor chamber (which forms a conduit for the passage of the primary jaw adductor muscles), a structure that scales with bite force (46).

The hyperossified vertebrate predators are largely isolated in a novel region of morphospace that includes distantly related species from 10 families and all microhabitat categories (Dataset S1 and Fig. 4, skulls 25 to 30). These taxa may have converged on a skull shape that enables them to withstand the high forces encountered when feeding on large, hard prey. Several of the hyperossified vertebrate predators with the most extreme skull shapes also possess odontoid fangs on the lower jaw [Fig. 2*C*; and sometimes on the palate (47)], which are tooth-like structures that enable the infliction of a bite-like wound and are thought to evolve in species that specialize on large prey (48). Odontoid fangs have also evolved in frogs that use male−male combat (e.g., *Adelotus*, *Limnonectes*), but these taxa lack hyperossification and do not occupy the hyperossified vertebrate predator morphospace. The only known anuran with true teeth on the lower jaw (*Gastrotheca guentheri*; point with dashed line in Fig. 2*C*, and ref. 22) occupies the same region of morphospace as the hyperossified vertebrate predators. There are no observations of this species consuming vertebrates in the wild, but *G. guentheri* will readily consume vertebrates in captivity and is known to consume large prey more than half of its body length (49).

Phragmotic Behavior. The species known to use phragmotic behavior occupy a novel region of morphospace that is characterized by an expansive skull roof (frontoparietals + nasals), resulting in a small dorsolateral window to the orbital cavity that enables these frogs to pull their eyes medially under the bony shelves for protection (Fig. 2, skull F and Fig. 4, skulls 19 to 24). At least four lineages have independently evolved this unique skull shape that is associated with phragmotic behavior—two clades of casque-headed hylids, *Peltophryne* toads, and *Gastrotheca galeata* (Fig. 1). Many of the casque-headed hylids and *Peltophryne* have been observed using phragmosis (29, 50), but the behavior is only hypothesized in *G. galeata* (51). All of these taxa are hyperossified, suggesting this extreme skull shape is achieved by hyperossification.

Phragmosis and the highly derived skulls of casque-headed hylids were originally hypothesized primarily to be an adaptation to prevent evaporative water loss while occupying tree holes,

bromeliads, rock crevices, or burrows in arid environments (14, 30, 52, 53). Recent work suggests these traits may also protect these animals against predators. Three phragmotic casque-headed hylid genera have been found to be venomous (*Aparasphenodon*, *Argenteohyla*, *Corythomantis*), with enlarged granular glands associated with the hyperossified spines of the skull that act as a venom delivery system (Fig. 4, skulls 20 and 21, and refs. 54–56). The remaining phragmotic species are not known to have this adaptation, but also have not been histologically investigated for similar glands. Phragmotic species have repeatedly evolved novel skull roof bones that are absent in all other frogs (internasal, dermal sphenethmoid, prenasal; refs. 29 and 57 and *SI Appendix*, Fig. S3), and these elements likely contribute to the extreme skull shape that these phragmotic species possess.

Hyperossification in Fossil Anurans. Hyperossification is common in anuran fossils (possibly because hyperossified elements are more likely to be preserved in the fossil record) and is present in putative archeobatrachians, mesobatrachians, and neobatrachians (58). Identifying the phylogenetic placement of these fossil taxa is challenging because the material is often fragmentary, and hyperossification seems to result in artificial groupings based on homoplastic features (44, 59, 60), despite the differences in shape identified across hyperossified species in our study. Our results corroborate these previous findings: Hyperossification likely has evolved multiple times across crown-group anurans, leading to increased rates of shape evolution. Additionally, many distantly related hyperossified lineages have converged on similar extreme skull shapes that may be linked to particular functions or behaviors. Including a broad taxonomic sample, using a molecular scaffold tree, conducting sensitivity analyses, and excluding or down-weighting characters possibly linked to hyperossification may eliminate some of these issues of homoplasy, but taxonomic uncertainty of these fossils will likely remain (60). Our framework will be useful in subsequent paleobiological studies of fossil frogs, especially when the 3D structure of the skull is recoverable. For example, *Baurubatrachus pricei* from the Late Cretaceous of Brazil (60), *Beelzebufo ampinga* from the Late Cretaceous of Madagascar (44), and *Thaumastosaurus gezei* from the Eocene of France (61) possess hyperossified, wide skulls with a posteriorly shifted jaw joint and bony articulation between the squamosal and maxilla, suggesting that these frogs specialized on eating relatively large, vertebrate prey.

Conclusions. Hyperossification has evolved in phylogenetically and ecologically diverse frog lineages and is repeatedly linked to the morphological expansion of the head into multiple novel shapes and functions. We find no support for a relationship between hyperossification and size. Microhabitat is correlated with skull shape but has a limited interaction with hyperossification. Several distantly related frogs that specialize in eating large, vertebrate prey have hyperossified skulls and converged on an extreme head shape that strengthens the skull and likely yields higher bite forces. A subset of the hyperossified vertebrate predators also have evolved odontoid fangs on the lower jaw convergently, enabling them to inflict a bite-like wound on prey. Phragmosis and an extreme skull shape are closely associated with one another and only cooccur when hyperossification is present. These traits facilitate a venom delivery system in a subset of phragmotic species to protect these animals against predators and may act as a barrier to avoid desiccation in others. Hyperossification is present in some anuran species that do not feed on large prey or use phragmotic behavior, and it is possible that, in these taxa, the function of hyperossification, if any, may be tied to osmoregulation. In addition to better exploring the interactions of skull shape, hyperossification, and water balance, a future avenue of research is to investigate whether cranium size and degree of ossification impacts the locomotor abilities of anurans. Our study demonstrates

the multifaceted relationship between skull shape, hyperossification, and ecology in frogs and highlights the importance of basic natural history data to identify the mechanisms responsible for generating macroevolutionary patterns of complex phenotypes.

Material and Methods

Sampling and Computed Tomography. For morphological comparisons and statistical analyses, we sampled nearly all hyperossified frog genera reported from the literature (reviewed in refs. 14 and 22), sister lineages to these genera that lack cranial hyperossification, and at least one representative from each of the 54 described anuran families (Dataset S1). Hyperossification was identified using the primary condition of exostosis (reticulate or pitting pattern; ref. 14). We performed high-resolution X-ray computed tomography scanning at the University of Florida's Nanoscale Research Facility, using a Phoenix v|tome|x M (GE Measurement & Control Solutions; *SI Appendix*). We deposited image stacks (TIFF) and 3D mesh files (STL) in MorphoSource (Dataset S1).

Ancestral State Reconstructions. We conducted ancestral state reconstructions of hyperossification in extant anurans using the presence/absence data collected from 158 anuran species (representing 145 genera and all 54 families) and the phylogeny of Jetz and Pyron (32). Bayesian ancestral state reconstructions were calculated using reversible-jump MCMC in RevBayes (34) to sample all five Markov models of phenotypic character evolution (one-rate, two-rate, zero-to-one irreversible, one-to-zero irreversible, no change) in proportion to their posterior probability (*SI Appendix*). We compared model fit using Bayes factors and accounted for model uncertainty by making model-averaged ancestral state estimates (refs. 62 and 63 and *SI Appendix*).

Shape Analyses. We obtained high-fidelity shape files for 158 species, each represented by one specimen. We quantified interspecific shape variation of the skull using 3D geometric morphometric analyses in the R package geomorph version 3.0.3 (33). Thirty-six fixed landmarks were digitized on each shape file, corresponding to homologous and repeatable points (*SI Appendix*, Fig. S1). A generalized Procrustes analysis was performed to align, rotate, and scale specimen landmark data to a common coordinate system and unit centroid size to remove variation in position, orientation, and size (64). A principal component analysis of skull shape variation was performed, and the Procrustes-aligned specimens were plotted in three dimensions of tangent space (PC1, PC2, and PC3). All of the following analyses were run for 10,000 iterations for significance testing. The pruned phylogeny of Jetz and Pyron (32) provided an estimate of evolutionary relationships for phylogenetic comparative methods.

To characterize skull diversity among all frog families more effectively, we tested for phylogenetic signal in skull shape and centroid size. The evolution of skull shape was visualized by estimating the maximum likelihood ancestral states of PC2 using the function contMap in the package phytools (65). We performed a phylogenetic MANOVA to test whether mean shape differed between hyperossified and nonhyperossified taxa. We estimated morphological disparity and net rates of skull shape evolution for hyperossified and nonhyperossified species to test whether there is a significant difference in Procrustes variance and morphological evolutionary rates between these two groups (66). To examine the relationship between skull centroid size and shape, we conducted a phylogenetic regression. A phylogenetic MANOVA and homogeneity of slopes test were conducted to test whether a significant interaction exists between hyperossification and centroid size and whether allometric slopes differ between hyperossified and nonhyperossified frogs. We used phylogenetic MANOVAs to test whether there are associations among microhabitat use, feeding biology, phragmotic behavior, and skull shape, as well as to determine whether there are significant interactions with hyperossification after accounting for main effects (*SI Appendix*). Microhabitat use (aquatic, arboreal, fossorial, and terrestrial), feeding biology (invertebrate predator, vertebrate predator), and phragmotic behavior (present, absent) data were collected from the literature (see Dataset S1 for references). The presence of odontoid fangs on the lower jaw was recorded for all species from computed tomography data.

Data Availability Statement. Computed tomography data (tiff stacks and mesh files) have been deposited in MorphoSource (see Dataset S1 for DOIs). Data and scripts for all analyses are available on GitHub at https://github.com/dpaluh/hyperossification.

1. S. Wroe, N. Milne, Convergence and remarkably consistent constraint in the evolution of carnivore skull shape. *Evolution* **61**, 1251–1260 (2007).
2. D. Schluter, Adaptive radiation in sticklebacks: Size, shape, and habitat use efficiency. *Ecology* **74**, 699–709 (1993).
3. M. H. Wake, "The skull as a locomotor organ" in *The Skull*, J. Hanken, B. K. Hall, Eds. (University of Chicago Press, 1993), vol. 3, pp. 197–240.
4. A. Herrel, E. De Grauw, J. A. Lemos-Espinal, Head shape and bite performance in xenosaurid lizards. *J. Exp. Zool.* **290**, 101–107 (2001).
5. J. S. Morris, D. R. Carrier, Sexual selection on skeletal shape in Carnivora. *Evolution* **70**, 767–780 (2016).
6. A. Herrel, V. Schaerlaeken, J. J. Meyers, K. A. Metzger, C. F. Ross, The evolution of cranial design and performance in squamates: Consequences of skull-bone reduction on feeding behavior. *Integr. Comp. Biol.* **47**, 107–117 (2007).
7. F. C. Barros, A. Herrel, T. Kohlsdorf, Head shape evolution in Gymnophthalmidae: Does habitat use constrain the evolution of cranial design in fossorial lizards? *J. Evol. Biol.* **24**, 2423–2433 (2011).
8. S. B. Emerson, D. M. Bramble, "Scaling, allometry, and skull design" in *The Skull*, J. Hanken, B. K. Hall, Eds. (University of Chicago Press, 1985), vol. 3, pp. 384–421.
9. M. Vidal-García, J. Scott Keogh, Phylogenetic conservatism in skulls and evolutionary lability in limbs—Morphological evolution across an ancient frog radiation is shaped by diet, locomotion and burrowing. *BMC Evol. Biol.* **17**, 165 (2017).
10. J. Hanken, B. K. Hall, *The Skull* (University of Chicago Press, 1993), vol. 2.
11. G. B. Müller, G. P. Wagner, Novelty in evolution: Restructuring the concept. *Annu. Rev. Ecol. Evol. Syst.* **22**, 229–256 (1991).
12. M. K. Vickaryous, J.-Y. Sire, The integumentary skeleton of tetrapods: Origin, evolution, and development. *J. Anat.* **214**, 441–464 (2009).
13. V. de Buffrénil, F. Clarac, A. Canoville, M. Laurin, Comparative data on the differentiation and growth of bone ornamentation in gnathostomes (Chordata: Vertebrata). *J. Morphol.* **277**, 634–670 (2016).
14. L. Trueb, "Bones, frogs, and evolution" in *Evolutionary Biology of the Anurans: Contemporary Research on Major Problems*, J. L. Vlal, Ed. (University of Missouri Press, 1973), pp. 65–132.
15. P. Alberch, S. J. Gould, G. F. Oster, D. B. Wake, Size and shape in ontogeny and phylogeny. *Paleobiology* **5**, 296–317 (1979).
16. C. J. Law, Evolutionary shifts in extant mustelid (Mustelidae: Carnivora) cranial shape, body size and body shape coincide with the Mid-Miocene Climate Transition. *Biol. Lett.* **15**, 20190155 (2019).
17. F. Clarac *et al.*, Does skull morphology constrain bone ornamentation? A morphometric analysis in the Crocodylia. *J. Anat.* **229**, 292–301 (2016).
18. P. L. Godoy, Crocodylomorph cranial shape evolution and its relationship with body size and ecology. *J. Evol. Biol.* **33**, 4–21 (2020).
19. G. R. Handrigan, R. J. Wassersug, The anuran Bauplan: A review of the adaptive, developmental, and genetic underpinnings of frog and tadpole morphology. *Biol. Rev. Camb. Philos. Soc.* **82**, 1–25 (2007).
20. W. E. Duellman, The numbers of amphibians and reptiles. *Herpetol. Rev.* **10**, 83–84 (1979).
21. University of California, Berkeley, AmphibiaWeb: Information on amphibian biology and conservation. https://amphibiaweb.org/. Accessed 12 February 2020.
22. W. E. Duellman, L. Trueb, *Biology of Amphibians* (McGraw-Hill, 1986).
23. D. R. Frost *et al.*, The amphibian tree of life. *Bull. Am. Mus. Nat. Hist.* **297**, 8–370 (2006).
24. Y. J. Feng *et al.*, Phylogenomics reveals rapid, simultaneous diversification of three major clades of Gondwanan frogs at the Cretaceous–Paleogene boundary. *Proc. Natl. Acad. Sci. U.S.A.* **114**, E5864–E5870 (2017).
25. L. Trueb, P. Alberch, "Miniaturization and the anuran skull: A case study of heterochrony" in *Functional Morphology in Vertebrates*, H. R. Duncker, G. Fleischer, Eds. (Gustav Fischer Verlag, 1985), pp. 113–121.
26. S. B. Emerson, Skull shape in frogs–Correlations with diet. *Herpetologica* **1985**, 177–188 (1985).
27. L. Trueb, "Patterns of cranial diversity among the Lissamphibia" in *The Skull*, J. Hanken, B. K. Hall, Eds. (University of Chicago Press, 1993), vol. 2, pp. 255–343.
28. K. D. Wells, *The Ecology and Behavior of Amphibians* (University of Chicago Press, 2007).
29. L. Trueb, Evolutionary relationships of casque-headed tree frogs with co-ossified skulls (family Hylidae). *Univ. Kans. Publ. Mus. Nat. Hist.* **18**, 547–716 (1970).
30. E. A. Seibert, H. B. Lillywhite, R. J. Wassersug, Cranial coossification in frogs: Relationship to rate of evaporative water loss. *Physiol. Zool.* **47**, 261–265 (1974).
31. J. Hanken, "Adaptation of bone growth to miniaturization of body size" in *Bone*, B. K. Hall, Ed. (CRC Press, 1993), vol. 7, pp. 79–104.

EVOLUTION

32. W. Jetz, R. A. Pyron, The interplay of past diversification and evolutionary isolation with present imperilment across the amphibian tree of life. *Nat. Ecol. Evol.* **2**, 850–858 (2018).

33. D. C. Adams, E. Otarola-Castillo, geomorph: an R package for the collection and analysis of geometric morphometric shape data. *Methods Ecol. Evol.* **4**, 393–399 (2013).

34. S. Höhna *et al.*, RevBayes: Bayesian phylogenetic inference using graphical models and an interactive model-specification language. *Syst. Biol.* **65**, 726–736 (2016).

35. J. Yeh, The effect of miniaturized body size on skeletal morphology in frogs. *Evolution* **56**, 628–641 (2002).

36. L. Trueb, L. A. Púgener, A. M. Maglia, Ontogeny of the bizarre: An osteological description of *Pipa pipa* (Anura: Pipidae), with an account of skeletal development in the species. *J. Morphol.* **243**, 75–104 (2000).

37. E. Fernandez, F. Irish, D. Cundall, How a frog, *Pipa pipa*, succeeds or fails in catching fish. *Copeia* **105**, 108–119 (2017).

38. D. Cundall, E. Fernandez, F. Irish, The suction mechanism of the pipid frog, *Pipa pipa* (Linnaeus, 1758). *J. Morphol.* **278**, 1229–1240 (2017).

39. E. Ascarrunz, J. C. Rage, P. Legreneur, M. Laurin, *Triadobatrachus massinoti*, the earliest known lissamphibian (Vertebrata: Tetrapoda) re-examined by μCT-Scan, and the evolution of trunk length in batrachians. *Contrib. Zool.* **85**, 201–234 (2016).

40. N. H. Shubin, F. A. Jenkins Jr, An Early Jurassic jumping frog. *Nature* **377**, 49–52 (1995).

41. A. M. Báez, N. Basso, The earliest known frogs of the Jurassic of South America: Review and cladistic appraisal of their relationships. *Münch. Geowiss. Abh. A* **30**, 131–158 (1996).

42. K.-Q. Gao, Y. Wang, Mesozoic anurans from Liaoning Province, China, and phylogenetic relationships of archaeobatrachian anuran clades. *J. Vertebr. Paleontol.* **21**, 460–476 (2001).

43. S. M. Reilly, E. O. Wiley, D. J. Meinhardt, An integrative approach to heterochrony: The distinction between interspecific and intraspecific phenomena. *Biol. J. Linn. Soc. Lond.* **60**, 119–143 (1997).

44. S. E. Evans, J. R. Groenke, M. E. H. Jones, A. H. Turner, D. W. Krause, New material of *Beelzebufo*, a hyperossified frog (Amphibia: Anura) from the Late Cretaceous of Madagascar. *PLoS One* **9**, e87236 (2014).

45. B. R. Scheffers *et al.*, Increasing arboreality with altitude: A novel biogeographic dimension. *Proc. Biol. Sci.* **280**, 20131581 (2013).

46. A. K. Lappin *et al.*, Bite force in the horned frog (*Ceratophrys cranwelli*) with implications for extinct giant frogs. *Sci. Rep.* **7**, 11963 (2017).

47. C. A. Sheil, J. R. Mendelson, III, A new species of *Hemiphractus* (Anura: Hylidae: Hemiphractinae), and a redescription of *H. johnsoni*. *Herpetologica* **57**, 189–202 (2001).

48. M. Fabrezi, S. B. Emerson, Parallelism and convergence in anuran fangs. *J. Zool. (Lond.)* **260**, 41–51 (2003).

49. D. J. Paluh, E. L. Stanley, D. C. Blackburn, First dietary record of *Gastrotheca guentheri* (Boulenger, 1882), the lone anuran with true mandibular teeth. *Herpetol. Notes* **12**, 699–700 (2019).

50. J. B. Pramuk, Prenasal bones and snout morphology in West Indian bufonids and the *Bufo granulosus* species group. *J. Herpetol.* **34**, 334–340 (2000).

51. L. Trueb, W. E. Duellman, An extraordinary new casque-headed marsupial frog (Hylidae: Gastrotheca). *Copeia* **1978**, 498–503 (1978).

52. D. V. de Andrade, A. S. Abe, Evaporative water loss and oxygen uptake in two casque-headed tree frogs, *Aparasphenodon brunoi* and *Corythomantis greeningi* (Anura, Hylidae). *Comp. Biochem. Physiol. A Physiol.* **118**, 685–689 (1997).

53. C. A. Navas, C. Jared, M. M. Antoniazzi, Water economy in the casque-headed tree-frog *Corythomantis greeningi* (Hylidae): Role of behaviour, skin, and skull skin co-ossification. *J. Zool. (Lond.)* **257**, 525–532 (2002).

54. C. Jared *et al.*, Venomous frogs use heads as weapons. *Curr. Biol.* **25**, 2166–2170 (2015).

55. C. Jared *et al.*, Head co-ossification, phragmosis and defence in the casque-headed tree frog *Corythomantis greeningi*. *J. Zool. (Lond.)* **265**, 1–8 (2005).

56. R. Cajade *et al.*, Multiple anti-predator mechanisms in the red-spotted Argentina Frog (Amphibia: Hylidae). *J. Zool. (Lond.)* **302**, 94–107 (2017).

57. S. A. Smith, S. Arif, A. N. de Oca, J. J. Wiens, A phylogenetic hot spot for evolutionary novelty in Middle American treefrogs. *Evolution* **61**, 2075–2085 (2007).

58. B. Sanchíz, *Handbuch der Paläoherpetologie. Part 4. Salientia* (Verlag Friedrich Pfeil, 1998).

59. S. Ruane, R. A. Pyron, F. T. Burbrink, Phylogenetic relationships of the Cretaceous frog *Beelzebufo* from Madagascar and the placement of fossil constraints based on temporal and phylogenetic evidence. *J. Evol. Biol.* **24**, 274–285 (2011).

60. A. M. Báez, R. O. Gómez, Dealing with homoplasy: Osteology and phylogenetic relationships of the bizarre neobatrachian frog *Baurubatrachus pricei* from the Upper Cretaceous of Brazil. *J. Syst. Paleontol.* **16**, 279–308 (2018).

61. F. Laloy *et al.*, A re-interpretation of the Eocene anuran *Thaumastosaurus* based on microCT examination of a 'mummified' specimen. *PLoS One* **8**, e74874 (2013).

62. W. A. Freyman, S. Höhna, Cladogenetic and anagenetic models of chromosome number evolution: A Bayesian model averaging approach. *Syst. Biol.* **67**, 195–215 (2018).

63. F. D. Freund, W. A. Freyman, C. J. Rothfels, Inferring the evolutionary reduction of corm lobation in *Isoëtes* using Bayesian model-averaged ancestral state reconstruction. *Am. J. Bot.* **105**, 275–286 (2018).

64. F. J. Rohlf, D. E. Slice, Extensions of the Procrustes method for the optimal superimposition of landmarks. *Syst. Zool.* **39**, 40–59 (1990).

65. L. J. Revell, phytools: An R package for phylogenetic comparative biology (and other things). *Methods Ecol. Evol.* **3**, 217–223 (2012).

66. D. C. Adams, Quantifying and comparing phylogenetic evolutionary rates for shape and other high-dimensional phenotypic data. *Syst. Biol.* **63**, 166–177 (2014).

67. A. Eklund, Beeswarm: The Bee Swarm Plot, an Alternative to Stripchart, R package Version 0.2. 3. http://www.cbs.dtu.dk/~eklund/beeswarm/. Accessed 22 December 2019.